Environmental Science Nano

ROYAL SOCIETY OF CHEMISTRY

COMMUNICATION

View Article Online
View Journal | View Issue

Check for updates

Cite this: *Environ. Sci.: Nano*, 2021, **8**, 1536

Received 2nd January 2021,
Accepted 12th May 2021

DOI: 10.1039/d1en00002k

rsc.li/es-nano

Emerging investigator series: aramid amphiphile nanoribbons for the remediation of lead from contaminated water†

Ty Christoff-Tempesta and Julia H. Ortony *

Self-assembled nanoribbons from small molecule amphiphiles with a structural domain to impart mechanical stability and chelating head groups are reported for the remediation of lead from contaminated water. The nanoribbons' remediation capacity is affected by pH and the presence of competing cations, and can be modulated by head group choice.

Small molecule amphiphiles self-assemble in water to form nanostructures that exhibit high surface areas and tuneable surface chemistries, and are readily scalable.[1–5] These properties have led to their extensive investigation as a platform for biomedical applications, including as materials for regenerative medicine, drug delivery, or biosensing.[6–8] In these environments, the dynamic nature of small molecule assemblies is harnessed as a design feature to mimic those of natural systems.[9–11,42] Such dynamics further enable the sensitivity of molecular assemblies to changes in their solvent environments, such as fluctuations in pH or temperature.[12,13] However, this property limits their application space to intentionally dynamic materials.

Molecular self-assembly could offer notable advantages to applications in non-biological contexts if their typical dynamic instabilities were overcome. In particular, self-assembled nanomaterials may provide a new strategy for point-of-use remediation of contaminants from drinking water. Surface areas on the order of hundreds of $m^2\ g^{-1}$ – resulting from nanostructure length scales determined by the length of the constituent amphiphiles[1,14] – may provide a platform for sequestering heavy metals. Namely, these nanostructure surfaces could be entirely coated with moieties capable of heavy metal remediation by presenting a hydrophilic chelator on every molecule. Realizing this design rationale requires the suppression of amphiphile exchange to minimize the rearrangement and release of amphiphile molecules from their assembled structures into the solvent space. Suppression of these exchange dynamics may also reduce the sensitivity of the assembly to variations in its environment such and temperature and pH.[15]

The removal of lead ions, Pb^{2+}, from drinking water is a critical target. Inorganic lead is a potent toxin which can damage nearly all organs, with adverse health effects including neurotoxicity, cardiovascular complications, cancer, and death.[16,17] Lead enters drinking water from a variety of sources, including the production and disposal of lead-acid batteries, alloy manufacturing, and, particularly, the erosion of plumbing.[18–20] Lead contamination crises persist globally, and increasing research indicates these events disproportionately occur in the United States along racial and socioeconomic lines.[21–24] Thus, there exists an urgent need to develop contemporary strategies for point-of-use remediation of lead from drinking water streams.

Here, we present the design of small molecule amphiphiles which exhibit three characteristics for the remediation of lead from contaminated water (Fig. 1): (1) amphiphilicity to induce spontaneous self-assembly in water into high surface area nanostructures; (2) a structural domain to provide intermolecular cohesion; and (3) a chelating head

Environmental significance

Lead poisoning causes over one million deaths annually, leading to the designation of lead as one of the World Health Organization's "ten chemicals of major public health concern". To address this crisis, high surface area nanomaterials offer promise for producing miniaturized technologies capable of effective lead remediation. We present small molecules that spontaneously self-assemble in water to form nanoribbons with lead-chelating surface groups. While supramolecular nanostructures are typically fragile, we incorporate hydrogen bonding aramid domains to suppress exchange dynamics, ultimately leading to nanoribbons with structural integrity. We demonstrate that design of small molecules is a route to new ion-selective chelating nanomaterials with tunable surface chemistries, and thereby demonstrate the potential of small molecule self-assembly for heavy metal remediation.

Department of Materials Science and Engineering, Massachusetts Institute of Technology, Cambridge, MA 02139, USA. E-mail: ortony@mit.edu

† Electronic supplementary information (ESI) available: Synthesis and experimental details, Fig. S1–S7. See DOI: 10.1039/d1en00002k

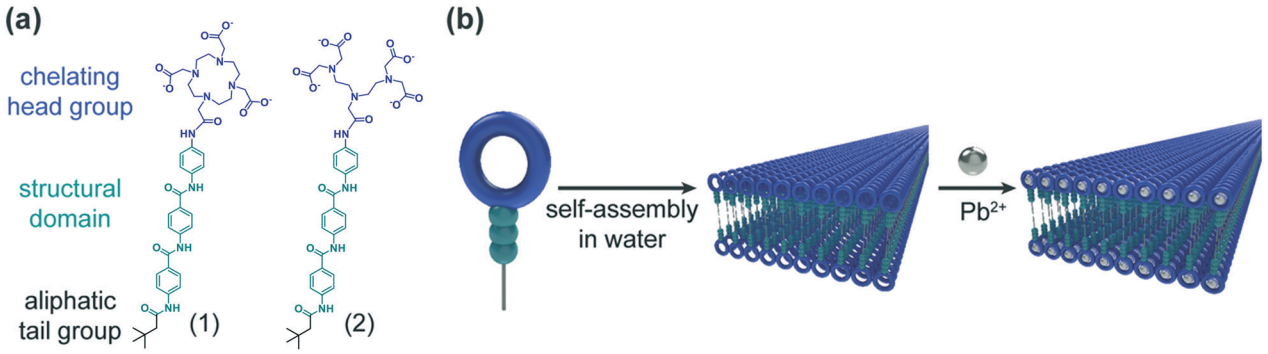

Fig. 1 Aramid amphiphiles with a heavy metal chelating head group self-assemble into nanoribbons for the remediation of lead from contaminated water. (a) Aramid amphiphiles contain an aliphatic, nonpolar tail group (black) and hydrophilic head group (purple) to induce self-assembly *via* the hydrophobic effect. A structural domain (turquoise) imparts structural stability to the assembled nanostructure. To chelate Pb^{2+} from water, head groups are selected with a DOTA (compound **1**) or DTPA (compound **2**) moiety. (b) Aramid amphiphiles spontaneously self-assemble upon the addition of water to form Pb^{2+}-chelating nanoribbons.

group capable of strongly binding to heavy metal cations in solution. To accomplish these goals, we use the aramid amphiphile (AA) motif as the platform for molecular self-assembly.[25,43] AAs take advantage of a dense hydrogen bonding network to impart structural stability on assembled nanoribbons with surface areas on the order of 200 $m^2\ g^{-1}$. Of particular note for this application, the amphiphiles exhibit suppressed exchange dynamics upon assembly, hindering the release of amphiphiles from their nanostructure. The supressed exchange dynamics differentiate this self-assembly approach from those that have been previously explored for water treatment.[26,27] In previous reports, heavy metal cations initiate physical crosslinking that induces hydrogelation – a process that may impede surface chelation events by limiting diffusion to the inside of the gel.[28] This design presents advantages over other soft materials systems, including polymers and polymer networks, because: (1) all chemical groups responsible for heavy metal remediation are expressed on the nanostructure surfaces, and are thermodynamically prohibited from being buried within a material; (2) surface chemistries and functionalities can be readily tuned through careful selection of the hydrophilic head group, enabling tuning of heavy metal remediation effectiveness and selectivity; and (3) the chemical character of the chelating compounds is minimally impacted by requiring only one covalent tether to the nanostructure surface, maximizing ionic interactions with dissolved lead species.

We designed and synthesized two AAs for the remediation of heavy metals from drinking water: compound **1**, an AA with a DOTA (dodecane tetraacetic acid; also known as tetraxetan) head group, and compound **2**, an AA with a DTPA (diethylenetriaminepentaacetic acid; also known as pentetic acid) head group (Fig. 1a). These groups were selected for their high binding affinity to lead ions in solution and their capability of inducing amphiphilic self-assembly by providing sufficient head group hydrophilicity (Fig. 1b). Both AAs with DOTA and DTPA head groups harness ionic interactions from charged carboxylic acid moieties and dipole interactions from tertiary amines to sequester lead ions from water.[29,30] Compounds **1** and **2** were obtained by alternating carbodiimide-mediated amidation reactions and standard deprotection reactions. Synthesis details and characterization of the final compounds and their intermediates are provided in ESI† section 1.

We observe the spontaneous assembly of both compounds **1** and **2** in water into nanoribbons with lengths extending at least several microns (Fig. 2a and c) by transmission electron microscopy (TEM). To ascertain cross-sectional dimensions, we use cryogenic TEM (Cryo-TEM) to obtain high-resolution images of the nanoribbons in a solvated state and

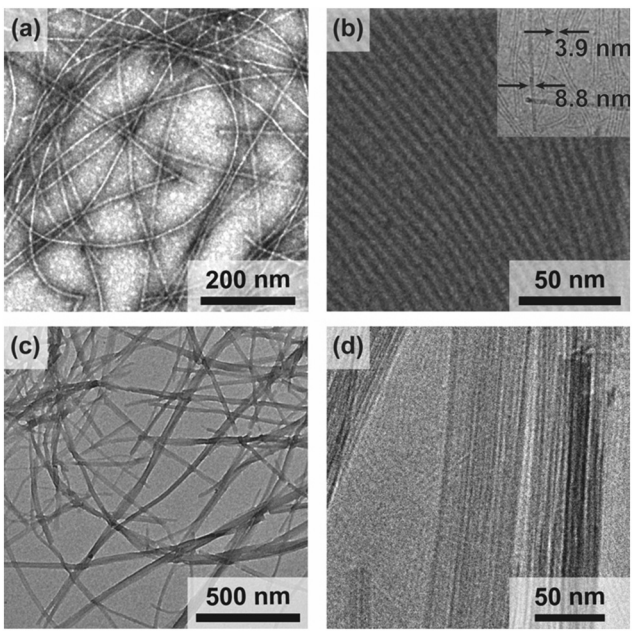

Fig. 2 Compounds **1** and **2** self-assemble into high aspect ratio nanoribbons in water. (a) Conventional TEM of **1** illustrates its assembly into microns-long nanoribbons. (b) Cryogenic TEM of **1** reveals a 3.9 nm × 8.8 nm nanoribbon cross-section (inset). (c) Conventional TEM of **2** shows bundling of microns-long nanoribbons. (d) Cryogenic TEM of **2** nanoribbons identifies a 3.9 × 5.1 nm cross-section.

synchrotron small angle X-ray scattering (SAXS) for nanostructure characterization. From these techniques, we find a 3.9 nm thickness and 8.8 nm width for compound **1**, and a 3.9 nm thickness by 5.1 nm width for compound **2** (Fig. 2b and d and ESI† Fig. S1). These dimensions give rise to surfaces areas on the order of 200 $m^2\ g^{-1}$.[25]

Having identified the geometries of the self-assembled nanostructures, we use a variety of techniques to characterize the chelation performance of compound **1** nanoribbons. Ultraviolet-visible (UV-vis) absorption spectroscopy allows us to observe the formation of the DOTA-lead complex.[31] An absorption peak at λ = 262 nm, characteristic of this complex, emerges as lead ions are titrated into a solution of compound **1** nanoribbons (Fig. 3a). The rise of this peak plateaus at 50 mol% Pb^{2+}, most likely signifying a 2 : 1 complexation of DOTA to the lead ions. This sandwich-type complex has been previously observed in similar systems where cyclic chelating moieties are maintained in close proximity.[32]

We employ isothermal titration calorimetry (ITC) to quantify thermodynamic parameters of the lead-binding surface reaction (Fig. 3b). This experiment captures the heat released from the injection of a concentrated lead solution into a dilute nanoribbon suspension. Injection of the concentrated lead solution into nanoribbon-free water is background-subtracted from this data to remove the heat of dilution. Negligible signal is detected by the injection of water into the nanoribbon suspension. From fitting sigmoidal curves to n = 3 runs, we calculate an equilibrium binding constant K_b = 2.2 ± 0.5 × 10^5 M^{-1}. This value indicates an equilibrium which strongly prefers the binding of lead ions to the nanoribbon surfaces, rather than the presence of lead ions free in solution, and implies that the nanoribbons are successful in remediating the heavy metal from contaminated water. This equilibrium constant further suggests that compound **1** nanoribbons should be used in significant excess to the lead present in contaminated water to thermodynamically drive remediation below the 15 ppb regulatory level for toxicity.[16] We further observe the plateau of chelation signal at n = 0.5, corroborating the saturation of the nanoribbons at 50 mol% Pb, and that the nanoribbons maintain their morphology after lead chelation (ESI† Fig. S2).

We hypothesize that the remediation capacity of lead ions by AA nanoribbons should be affected by pH, as protonation of the nanoribbon head groups would hinder ionic interactions between the chelating moieties and lead ions.[33] Because lead species become insoluble in basic environments,[34] we selected pH values of 7, 5, and 3 to test remediation capacity. We observe no change in assembly morphology of compound **1** nanoribbons when the pH is adjusted to 3 post-assembly (ESI† Fig. S3), likely because of the stability imparted to the structure by the aramid domain.

Adsorption isotherm curves are constructed for the uptake of lead by compound **1** nanoribbons to test pH sensitivity (Fig. 3c). Nanoribbons are mixed with Pb^{2+} 24 h before testing to ensure equilibrium is reached. Equilibrium data are fit to a Langmuir model, with R^2 values exceeding 0.97 in all cases (ESI† Fig. S4). Compound **1** nanoribbons demonstrate adsorption capacities (Q_o) of 72, 61, and 45 mg g^{-1} at pH values of 7, 5, and 3, respectively. As predicted, the lead chelation capacity drops slightly when changing from pH 7 to 5, and drops significantly at pH 3.

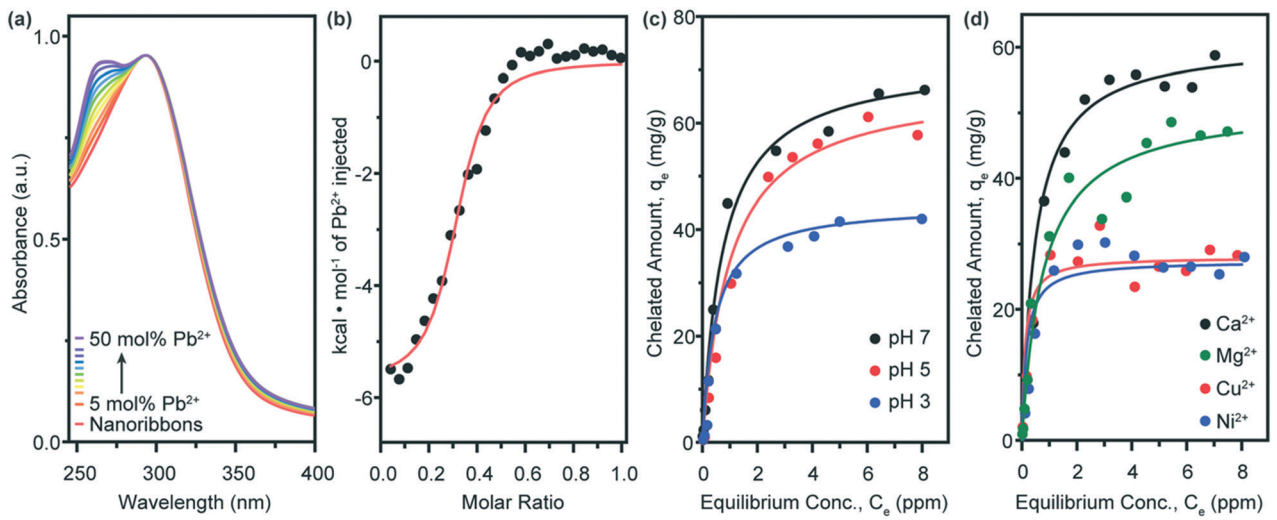

Fig. 3 Compound **1** nanoribbons remediate Pb^{2+} from water, exhibiting sensitivity to pH and the presence of competing divalent cations. (a) UV-vis absorption spectra show the appearance of a peak at λ = 262 nm, corresponding to the binding of Pb^{2+} to compound **1** nanoribbon DOTA groups. This peak intensity plateaus at 50 mol% Pb^{2+}, indicating a 2 : 1 amphiphile : Pb^{2+} stoichiometry of binding. (b) ITC reveals an equilibrium binding constant K_b = 2.2 ± 0.5 × 10^5 M^{-1} of Pb^{2+} to compound **1** nanoribbons, while further corroborating a 2 : 1 amphiphile : Pb^{2+} stoichiometry. (c) Adsorption isotherms illustrate a drop in equilibrium Pb^{2+} saturation on the nanoribbons from Q_o = 72 mg g^{-1} at pH 7, to Q_o = 61 mg g^{-1} at pH 5, to Q_o = 45 mg g^{-1} at pH 3. (d) Adsorption isotherms with equimolar amounts of Pb^{2+} and either Ca^{2+}, Mg^{2+}, Cu^{2+}, or Ni^{2+} demonstrate lead saturation capacities of 61, 52, 32, and 27 mg g^{-1}, respectively.

We further expect that the nanoribbons' lead adsorption capacities is sensitive to the presence of other multivalent cations which could compete with lead to occupy the chelation complex. To test this hypothesis, we constructed adsorption isotherms with equimolar amounts of lead and either calcium, copper, magnesium, or nickel ions (Fig. 3d). Fits of the equilibrium data to a Langmuir model (ESI† Fig. S5) are used to extract lead adsorption capacities in the equimolar presence of each ion: for Ca^{2+}, $Q_{o,Pb^{2+}}$ = 61 mg g^{-1}; for Mg^{2+}, $Q_{o,Pb^{2+}}$ = 52 mg g^{-1}; for Cu^{2+}, $Q_{o,Pb^{2+}}$ = 32 mg g^{-1}; and for Ni^{2+}, $Q_{o,Pb^{2+}}$ = 27 mg g^{-1}. Thus, from least to most interference with Pb^{2+} binding to compound **1** nanoribbons, we observe the following trend: $Ca^{2+} < Mg^{2+} \ll Cu^{2+}, Ni^{2+}$. This trend largely follows the equilibrium binding constants of the ions to the free DOTA molecule in solution.[35] To put this data in perspective, remediating 1 L of water with 50 ppb Pb to below 15 ppb Pb at pH 7 requires approximately 690 μg of compound **1** nanoribbons in the absence of competing counterions, and 820, 960, 1560, and 1850 μg compound **1** nanoribbons in the presence of equimolar amounts of Pb^{2+} and Ca^{2+}, Mg^{2+}, Cu^{2+}, and Ni^{2+}, respectively. These results confirm that the lead-binding capacity of compound **1** nanoribbons is reduced by the presence of competing multivalent cations and suggests that this system may be used to simultaneously remove several contaminants from polluted water.

The capacity of amphiphilic nanoribbons to remediate heavy metal ions from water should be sensitive to the geometry and chemical structure of the head group.[33] Lead ions likely percolate into the head group domain of compound **1** to sandwich between neighbouring DOTA head groups. Conversely, the DTPA head group of compound **2** is prone to facing outwards from the nanoribbon core due to steric hinderance and has four carboxylic acids per molecule available for complexation. Therefore, we expect compound **2** nanoribbons to exhibit more effectively sequester Pb^{2+} from water than those of compound **1**.

The formation of a lead : amphiphile chelation complex on compound **2** nanoribbons is monitored by UV-vis absorption spectroscopy with the emergence of a peak at λ = 255 nm (Fig. 4a). We observe that compound **2** nanoribbons maintain their morphology with chelation (Fig. S2†) and, interestingly, find compound **2** nanoribbon chelators saturate near 50 mol% Pb. This effect may result from hydrogen bonding between head groups, which leads to the bundling of nanoribbons (Fig. 2c and d), reducing the effective accessible surface area. Compound **2** nanoribbons exhibit an equilibrium binding constant of $K_b = 7.1 \pm 1.6 \times 10^5$ M^{-1} in n = 3 background-subtracted ITC experiments (Fig. 4b). This binding constant is statistically significantly higher than that of compound **1**, and predicts that compound **2** nanoribbons should thus exhibit enhanced lead binding in adsorption isotherm experiments. As with compound **1** nanoribbons, this equilibrium constant also implies that achieving lead remediation below 15 ppb requires using a significant excess of compound **2** nanoribbons relative to the lead present in the water.[16]

As with compound **1**, the remediation capacity of compound **2** nanoribbons is expected to be sensitive to pH as head group protonation inhibits ionic interactions with lead ions (Fig. 4c and ESI† Fig. S6). Compound **2** nanoribbons are also demonstrated to maintain their nanostructure upon environmental adjustment to pH 3 (ESI† Fig. S3). At pH 7, compound **2** nanoribbons have an equilibrium saturation

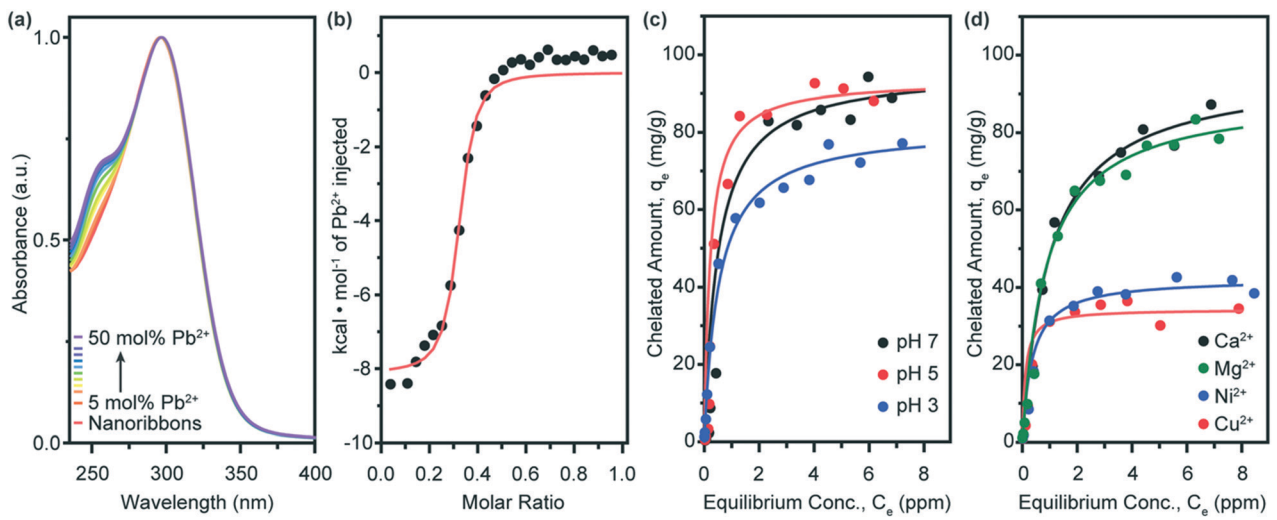

Fig. 4 Self-assembled compound **2** nanoribbons remediate higher quantities of lead from water than those of compound **1**. (a) UV-vis absorption spectra suggest 50% of all nanoribbon surfaces participate in Pb^{2+} binding from the plateau of an absorption peak at λ = 255 nm. (b) ITC, tracking heat released from the chelation of Pb^{2+}, reveals an equilibrium Pb^{2+} binding constant $K_b = 7.1 \pm 1.6 \times 10^5$ M^{-1}. (c) Adsorption isotherms demonstrate that decreasing pH leads to a decrease in equilibrium lead saturation of compound **2** nanoribbons from Q_o = 96 mg g^{-1} at pH 7, to Q_o = 93 mg g^{-1} at pH 5, to Q_o = 81 mg g^{-1} at pH 3. (d) Adsorption isotherm experiments with equimolar amounts of Pb^{2+} and either Ca^{2+}, Mg^{2+}, Ni^{2+}, or Cu^{2+} show equilibrium lead saturation capacities of 96, 90, 42, and 34 mg g^{-1}, respectively.

capacity of Q_o = 96 mg g^{-1}. This saturation capacity drops slightly to Q_o = 93 mg g^{-1} at pH 5, and further declines to Q_o = 81 mg g^{-1} at pH 3, following the expected trend and matching the pattern of compound **1**. Notably, the saturation capacity of compound **2** nanoribbons is higher than those of **1** across all pH values. This result, in conjunction with the elevated thermodynamic equilibrium binding constant of **2** nanoribbons, confirms that head group choice is a viable parameter for tuning chelation capacity of small molecule amphiphilic nanoribbons.

The saturation capacities of the nanoribbon materials presented here match or exceed those of functional materials investigated or in use today for lead remediation. For example, the equilibrium saturation capacities of compound **1** and **2** nanoribbons exceed that of activated carbon (50 mg g^{-1}),[36] sulfur-functionalized silica (46 mg g^{-1}),[37] acidified carbon nanotubes (17 mg g^{-1}),[38] and apricot stone (21 mg g^{-1}).[39] In contrast, compound **1** and **2** nanoribbons offer comparable performance to Fe(III)-modified zeolite (99 mg g^{-1})[40] and iron oxide nanomaterials (98 mg g^{-1}).[41]

Finally, we sought to identify the effect of competitive binding for chelation sites by divalent cations on compound **2** nanoribbons. We again performed adsorption isotherm experiments with equimolar amounts of lead and either calcium, copper, magnesium, or nickel ions (Fig. 4d and ESI† Fig. S7). For compound **2** nanoribbons, we find for Ca^{2+}, $Q_{o,Pb^{2+}}$ = 96 mg g^{-1}; for Mg^{2+}, $Q_{o,Pb^{2+}}$ = 90 mg g^{-1}; for Ni^{2+}, $Q_{o,Pb^{2+}}$ = 42 mg g^{-1}; and for Cu^{2+}, $Q_{o,Pb^{2+}}$ = 34 mg g^{-1}. From least to most interference with Pb^{2+} binding to **2** nanoribbons, we observe: $Ca^{2+} < Mg^{2+} \ll Ni^{2+} < Cu^{2+}$. These results indicate that remediating 1 L of water with 50 ppb Pb to below 15 ppb Pb at pH 7 requires approximately 520 μg of compound **2** nanoribbons in the absence of competing counterions, and 520, 560, 1190, and 1470 μg compound **2** nanoribbons in the presence of equimolar amounts of Pb^{2+} and Ca^{2+}, Mg^{2+}, Ni^{2+}, and Cu^{2+}, respectively. This trend generally follows that of equilibrium binding constants for these ions to free DTPA in solution.[35] Fractionally and in total saturation magnitude, compound **2** is affected less by competitive binding with these cations than compound **1**, with the exception of copper(II). This result suggests that head group choice can be used not only to improve adsorption capacity, but also to tune ion selectivity.

Conclusions

Here, we presented two aramid amphiphile (AA) molecules that spontaneously self-assemble in water, forming high-aspect-ratio nanoribbons, for the remediation of lead from contaminated water. Both AAs produced microns-long nanoribbons upon assembly with 4 nm × 5–9 nm cross-sections and surface areas on the order of hundreds of m^2 g^{-1}. All nanoribbons exhibited the capacity to capture Pb^{2+} with a 2 : 1 chelator : lead stoichiometry. Nanoribbons coated with a surface of DTPA chelators expressed a higher thermodynamic binding constant to lead than those with a DOTA surface, giving rise to higher equilibrium lead saturation capacities. The lead binding capacity of the supramolecular nanoribbons was sensitive to pH, dropping as the head groups became protonated with decreasing pH. The lead-binding efficacy of the nanoribbons was also impacted by the presence of other divalent cations which compete for chelation sites. This result indicates that AA nanoribbons may be used for the synergistic removal of multiple contaminants. Amphiphile head group choice was also identified as a parameter for optimizing binding efficacy and ion selectivity. The small molecule self-assembly strategy described here offers a paradigm for remediating contaminants from water that takes advantage of the high surface areas, tunable chemistries, and scalability of supramolecular nanostructures.

Author contributions

T. C.-T. and J. H. O. conceptualized the materials presented in this report. T. C.-T. performed the investigation and formal analysis in this manuscript. J. H. O. completed funding acquisition and supervision for the experiments described here. T. C.-T. and J. H. O. visualized the data and wrote the manuscript.

Conflicts of interest

There are no conflicts to declare.

Acknowledgements

The authors thank Edward J. Brignole and Phat Vinh Dip for their assistance with cryogenic transmission electron microscopy. T. C.-T. acknowledges the support of the National Science Foundation Graduate Research Fellowship Program under Grant No. 1122374 and the Martin Family Society of Fellows for Sustainability. This material is based upon work supported by the National Science Foundation under Grant No. CHE-194550. This work was supported in part by the Professor Amar G. Bose Research Grant Program, the Abdul Latif Jameel Water and Food Systems Lab, and the MIT Center for Environmental Health Sciences under NIH Center Grant P30-ES002109. This work made use of the MRSEC Shared Experimental Facilities at MIT, supported by the National Science Foundation under award number DMR-14-19807 and the MIT Department of Chemistry Instrumentation Facility. Specimens were prepared and imaged at the Automated Cryogenic Electron Microscopy Facility in MIT. nano on a Talos Arctica microscope, which was a gift from the Arnold and Mabel Beckman Foundation. X-ray scattering measurements were performed at beamline 12-ID-B of the Advanced Photon Source, a U.S. Department of Energy (DOE) Office of Science User Facility operated for the DOE Office of Science by Argonne National Laboratory under Contract No. DE-AC02-06CH11357.

References

1 G. M. Whitesides, J. P. Mathias and C. T. Seto, Molecular self-assembly and nanochemistry: a chemical strategy for the synthesis of nanostructures, *Science*, 1991, **254**, 1312–1319.
2 S. Zhang, Emerging biological materials through molecular self-assembly, *Biotechnol. Adv.*, 2002, **20**, 321–339.
3 C. Fong, T. Le and C. J. Drummond, Lyotropic liquid crystal engineering–ordered nanostructured small molecule amphiphile self-assembly materials by design, *Chem. Soc. Rev.*, 2012, **41**, 1297–1322.
4 A. Dasgupta and D. Das, Designer peptide amphiphiles: self-assembly to applications, *Langmuir*, 2019, **35**, 10704–10724.
5 S. J. Singer and G. L. Nicolson, The fluid mosaic model of the structure of cell membranes, *Science*, 1972, **175**, 720–731.
6 M. Rad-Malekshahi, L. Lempsink, M. Amidi, W. E. Hennink and E. Mastrobattista, Biomedical applications of self-assembling peptides, *Bioconjugate Chem.*, 2016, **27**, 3–18.
7 J. D. Hartgerink, E. Beniash and S. I. Stupp, Self-assembly and mineralization of peptide-amphiphile nanofibers, *Science*, 2001, **294**, 1684–1688.
8 N. Stephanopoulos, J. H. Ortony and S. I. Stupp, Self-assembly for the synthesis of functional biomaterials, *Acta Mater.*, 2013, **61**, 912–930.
9 S. Toledano, R. J. Williams, V. Jayawarna and R. V. Ulijn, Enzyme-triggered self-assembly of peptide hydrogels via reversed hydrolysis, *J. Am. Chem. Soc.*, 2006, **128**, 1070–1071.
10 R. Freeman, M. Han, Z. Álvarez, J. A. Lewis, J. R. Wester, N. Stephanopoulos, M. T. McClendon, C. Lynsky, J. M. Godbe and H. Sangji, Reversible self-assembly of superstructured networks, *Science*, 2018, **362**, 808–813.
11 R. J. Williams, A. M. Smith, R. Collins, N. Hodson, A. K. Das and R. V. Ulijn, Enzyme-assisted self-assembly under thermodynamic control, *Nat. Nanotechnol.*, 2009, **4**, 19–24.
12 A. D. Ozkan, A. B. Tekinay, M. O. Guler and E. D. Tekin, Effects of temperature, pH and counterions on the stability of peptide amphiphile nanofiber structures, *RSC Adv.*, 2016, **6**, 104201–104214.
13 J. D. Hartgerink, E. Beniash and S. I. Stupp, Peptide-amphiphile nanofibers: a versatile scaffold for the preparation of self-assembling materials, *Proc. Natl. Acad. Sci. U. S. A.*, 2002, **99**, 5133–5138.
14 L. C. Palmer and S. I. Stupp, Molecular self-assembly into one-dimensional nanostructures, *Acc. Chem. Res.*, 2008, **41**, 1674–1684.
15 S. E. Paramonov, H.-W. Jun and J. D. Hartgerink, Self-assembly of peptide– amphiphile nanofibers: the roles of hydrogen bonding and amphiphilic packing, *J. Am. Chem. Soc.*, 2006, **128**, 7291–7298.
16 M. J. Brown and S. Margolis, Lead in drinking water and human blood lead levels in the United States, Centers for Disease Control and Prevention, *Morb. Mortal. Wkly. Rep.*, 2012, **61**, 1–10.
17 M. Hauptman, R. Bruccoleri and A. D. Woolf, An update on childhood lead poisoning, *Clin. Pediatr. Emerg. Med.*, 2017, **18**, 181–192.
18 P. Levallois, P. Barn, M. Valcke, D. Gauvin and T. Kosatsky, Public health consequences of lead in drinking water, *Curr. Environ. Health Rep.*, 2018, **5**, 255–262.
19 E. Obeng-Gyasi, Sources of lead exposure in various countries, *Rev. Environ. Health*, 2019, **34**, 25–34.
20 T. Dignam, R. B. Kaufmann, L. LeStourgeon and M. J. Brown, Control of lead sources in the United States, 1970-2017: public health progress and current challenges to eliminating lead exposure, *J. Public Health Manag. Pract.*, 2019, **25**, S13.
21 F. Fernandez-Luqueno, F. López-Valdez, P. Gamero-Melo, S. Luna-Suárez, E. N. Aguilera-González, A. I. Martínez, M. García-Guillermo, G. Hernández-Martínez, R. Herrera-Mendoza and M. A. Álvarez-Garza, Heavy metal pollution in drinking water-a global risk for human health: A review, *Afr. J. Environ. Sci. Technol.*, 2013, **7**, 567–584.
22 T. M. Olson, M. Wax, J. Yonts, K. Heidecorn, S.-J. Haig, D. Yeoman, Z. Hayes, L. Raskin and B. R. Ellis, Forensic estimates of lead release from lead service lines during the water crisis in Flint, Michigan, *Environ. Sci. Technol. Lett.*, 2017, **4**, 356–361.
23 J. E. Johnston and A. Hricko, Industrial lead poisoning in Los Angeles: anatomy of a public health failure, *Environ. Justice*, 2017, **10**, 162–167.
24 R. J. Sampson and A. S. Winter, The racial ecology of lead poisoning: Toxic inequality in Chicago neighborhoods, 1995-2013, *Du Bois Rev.*, 2016, **13**, 261–283.
25 T. Christoff-Tempesta, D.-Y. Kim, Y. Cho, M. Geri, G. Lamour, A. J. Lew, X. Zuo, W. R. Lindemann and J. H. Ortony, Self-assembly of aramid amphiphiles into ultra-stable nanoribbons and aligned nanoribbon threads, *Nat. Nanotechnol.*, 2021, **16**, 447–454.
26 B. Mondal, D. Bairagi, N. Nandi, B. Hansda, K. S. Das, C. J. C. Edwards-Gayle, V. Castelletto, I. W. Hamley and A. Banerjee, Peptide-Based Gel in Environmental Remediation: Removal of Toxic Organic Dyes and Hazardous Pb2+ and Cd2+ Ions from Wastewater and Oil Spill Recovery, *Langmuir*, 2020, **36**, 12942–12953.
27 P. J. Knerr, M. C. Branco, R. Nagarkar, D. J. Pochan and J. P. Schneider, Heavy metal ion hydrogelation of a self-assembling peptideviacysteinyl chelation, *J. Mater. Chem.*, 2012, **22**, 1352–1357.
28 T. Christoff-Tempesta, A. J. Lew and J. H. Ortony, Beyond covalent crosslinks: applications of supramolecular gels, *Gels*, 2018, **4**, 40.
29 J. W. Nugent, H.-S. Lee, J. H. Reibenspies and R. D. Hancock, Spectroscopic, structural, and thermodynamic aspects of the stereochemically active lone pair on lead (II): Structure of the lead (II) dota complex, *Polyhedron*, 2015, **91**, 120–127.
30 V. L. Silva, R. Carvalho, M. P. Freitas, C. F. Tormena and W. C. Melo, Spectrometric and theoretical investigation of the structures of Cu and Pb/DTPA complexes, *Struct. Chem.*, 2007, **18**, 605–609.
31 A. Pasha, G. Tircsó, E. T. Benyó, E. Brücher and A. D. Sherry, Synthesis and characterization of DOTA-(amide) 4 derivatives:

equilibrium and kinetic behavior of their lanthanide (III) complexes, *Eur. J. Inorg. Chem.*, 2007, **2007**, 4340.

32 E. N. Ushakov, S. P. Gromov, O. A. Fedorova, Y. V. Pershina, M. V. Alfimov, F. Barigelletti, L. Flamigni and V. Balzani, Sandwich-type complexes of alkaline-earth metal cations with a bisstyryl dye containing two crown ether units, *J. Phys. Chem. A*, 1999, **103**, 11188–11193.

33 E. Deiss-Yehiely, J. H. Ortony, B. Qiao, S. I. Stupp and M. Olvera de la Cruz, Ion condensation onto self-assembled nanofibers, *J. Polym. Sci., Part B: Polym. Phys.*, 2017, **55**, 901–906.

34 M. R. Schock, I. Wagner and R. Oliphant, The corrosion and solubility of lead in drinking water, *Internal corrosion of water distribution systems*, 1996, vol. 4, pp. 131–230.

35 G. Anderegg, F. Arnaud-Neu, R. Delgado, J. Felcman and K. Popov, Critical evaluation of stability constants of metal complexes of complexones for biomedical and environmental applications*(IUPAC Technical Report), *Pure Appl. Chem.*, 2005, **77**, 1445–1495.

36 M. A. P. Cechinel and A. A. U. de Souza, Study of lead (II) adsorption onto activated carbon originating from cow bone, *J. Cleaner Prod.*, 2014, **65**, 342–349.

37 H.-T. Fan, J.-B. Wu, X.-L. Fan, D.-S. Zhang, Z.-J. Su, F. Yan and T. Sun, Removal of cadmium (II) and lead (II) from aqueous solution using sulfur-functionalized silica prepared by hydrothermal-assisted grafting method, *Chem. Eng. J.*, 2012, **198**, 355–363.

38 Y.-H. Li, S. Wang, J. Wei, X. Zhang, C. Xu, Z. Luan, D. Wu and B. Wei, Lead adsorption on carbon nanotubes, *Chem. Phys. Lett.*, 2002, **357**, 263–266.

39 L. Mouni, D. Merabet, A. Bouzaza and L. Belkhiri, Adsorption of Pb (II) from aqueous solutions using activated carbon developed from Apricot stone, *Desalination*, 2011, **276**, 148–153.

40 M. Kragović, A. Daković, M. Marković, J. Krstić, G. D. Gatta and N. Rotiroti, Characterization of lead sorption by the natural and Fe (III)-modified zeolite, *Appl. Surf. Sci.*, 2013, **283**, 764–774.

41 W. Chen, Z. Lu, B. Xiao, P. Gu, W. Yao, J. Xing, A. M. Asiri, K. A. Alamry, X. Wang and S. Wang, Enhanced removal of lead ions from aqueous solution by iron oxide nanomaterials with cobalt and nickel doping, *J. Cleaner Prod.*, 2019, **211**, 1250–1258.

42 J. H. Ortony, C. J. Newcomb, J. B. Matson, L. C. Palmer, P. E. Doan, B. M. Hoffman and S. I. Stupp, Internal dynamics of a supramolecular nanofibre, *Nat. Mater.*, 2014, **13**(8), 812–816.

43 W. R. Lindemann, T. Christoff-Tempesta and J. H. Ortony, A Global Minimization Toolkit for Batch-Fitting and $\chi 2$ Cluster Analysis of CW-EPR Spectra, *Biophys. J.*, 2020, **119**(10), 1937–1945.

